Synthesis, Structure and Characterization of a New Complex: $[Mn(C_6H_{12}N_4)_2(H_2O)_4][Mn(H_2O)_6][SO_4]_2\cdot 6H_2O$①

LI Deng-Peng[a, b] XU Zhi-Huang[b]
YE Li-Wang[b] CAO Teng-Fei[a, b] ZHUANG Xin-Xin[b②]
[a] (*College of Chemistry, Fuzhou University, Fuzhou* 350116, *China*)
[b] (*Key Laboratory of Optoelectronic Materials Chemistry and Physics, Fujian Institute of Research on the Structure of Matter, Chinese Academy of Sciences, Fuzhou* 350002, *China*)

ABSTRACT A novel complex, $[Mn(C_6H_{12}N_4)_2(H_2O)_4][Mn(H_2O)_6][SO_4]_2\ 6H_2O$, was synthesized and hexagonal single crystals with centimeter-scale sizes were obtained by the method of solvent evaporation. It was characterized by elemental analysis, infrared spectrum, thermogravimetric analysis and X-ray single-crystal diffraction. The complex belongs to triclinic crystal system, space group $P\bar{1}$ with a = 9.3390(8), b = 13.3520(13), c = 16.3207(13) Å, α = 100.7160(3)°, β = 90.1020(10)°, γ = 109.9490(5)°, V = 1874.9(3) Å^3, Z = 2, D_c = 1.542 g/cm^3, M_r = 870.64, μ = 0.876 mm^{-1}, T = 293(2) K, F(000) = 916 and S = 0.990. The crystal structure determination displayed a distorted octahedral geometry around the manganese atom, which is bound to two nitrogen atoms from hexamethylenetetramine, acting as monodentate ligands, and to four aqua ligands. Variable-temperature magnetic measurements of the complex indicate the presence of weak antiferromagnetic interaction between manganese centers.

Keywords: hexamethylenetetramine, crystal structure, thermal stability, susceptibility;
DOI: 10.14102/j.cnki.0254–5861.2011–3119

1 INTRODUCTION

Transition metal complexes have been synthesized and studied for decades due to their remarkable magnetic, spectroscopic and electrochemical properties[1-7]. Several transition metal ions, such as Mn(II), have shown a unique capacity to provide interesting magnetic properties by virtue of the spin motion of *d*-orbital unpaired electrons and their complexes have also been developed rapidly for the applications in paramagnetic resonance[8], probes[9-11] and contrast reagents[12-15]. The selection of organic ligands is the key factor affecting the structures and properties of these complexes[16]. Nitrogen or oxygen-containing ligands, such as hexamethylenetetramine, is not only structurally stable, but also shows the relatively strong binding affinity toward transition metal for the existence of nitrogen atoms with lone pair electrons. A series of transition metal complexes with hexamethylenetetramine as ligands, such as $[M(C_6H_{12}N_4)_2(H_2O)_4][M(H_2O)_6][SO_4]_2\ 6H_2O$ (M = Ni, Zn or Co), have been published[17-19]. But to the best of our knowledge, the synthesis, structure and properties of the Mn complex have not been reported systematically. Mn(Ⅱ) ion has the most *d*-orbital unpaired electrons compared with that of other transition metal ions, which makes its complex usually an interesting magnetic material. However, it's not easy to synthesize the corresponding manganese complex for the reason that the alkaline hexamethylenetetramine can oxidize Mn(Ⅱ) ions in aqua solution. Therefore, it's worthwhile to explore the synthesis methods and study its properties. Taking account of the above, we attempt to synthesize this transition metal with sulfuric acid additive.

In this paper, a new manganese complex with hexamethylenetetramine as ligands was reported and its single crystal was obtained by evaporation method. X-ray single-crystal diffraction measurements were applied to investigate its structure, thermogravimetric analysis and variable-temperature magnetic measurements were carried out to characterize its physical properties.

2 EXPERIMENTAL

Received 25 January 2021; accepted 15 March 2021 (**CCDC 2045333**)
① Supported by the Key Laboratory of Optoelectronic Materials Chemistry and Physics, Chinese Academy of Sciences
② Corresponding author. Researcher. E-mail: zxx@fjirsm.ac.cn

2. 1 Materials and physical instruments

All the materials and reagents were obtained commercially and used without further purification. TGA and DTA curves of the samples were tested with STA449F3 thermal analyzer. Carbon, nitrogen and hydrogen analysis were determined on a Vario EL-Cube element analyzer. IR spectra in the range of 4000~400 cm^{-1} were measured on a Vertex70 infrared spectrometer. X-ray powder diffraction experiments were conducted on a Miniflex600 Desktop X-ray Diffractometer with Cu*Kα* radiation. The MM007-Saturn724+ Small Molecule Single-Crystal X-ray Diffractometer was used for data collection. Magnetic susceptibility measurements were performed by a SQUID-VSM magnetometer.

2. 2 Synthesis of the complex

Hexamethylenetetramine (57.47 g, 0.41 mol) and monohydrate manganese sulfate (33.80 g, 0.2 mol) were respectively dissolved in water and the pH of manganese sulfate solution was adjusted to 4 with sulfuric acid additive. Hexamethylenetetramine solution was poured into the monohydrate manganese sulfate solution several times in small amounts, and the pH of the mixed solution was adjusted to 7.5 by sulfuric acid every time. The growth solution was evaporated at 30 ℃ for 72 hours to produce hexagonal transparent single crystals, as shown in Fig. 1(a) and 1(b). Elemental analysis calcd. for $C_{12}H_{56}N_8Mn_2O_{24}S_2$ (%): C, 16.56; H, 6.44; N, 12.88. Found (%): C, 16.33; H, 6.38; N, 12.55. Main IR frequencies (KBr, cm^{-1}): 3416, 2965, 1658, 1465, 1243, 1112, 1005, 809, 691, 615, 506.

Fig. 1(c) shows the precipitates of by-product in solution without sulfuric acid additive, which seriously degrade the quality of crystallization. PXRD measurement carried out on the collected by-product revealed the formation of oxidation product Mn_3O_4 (Fig. 1(d)).

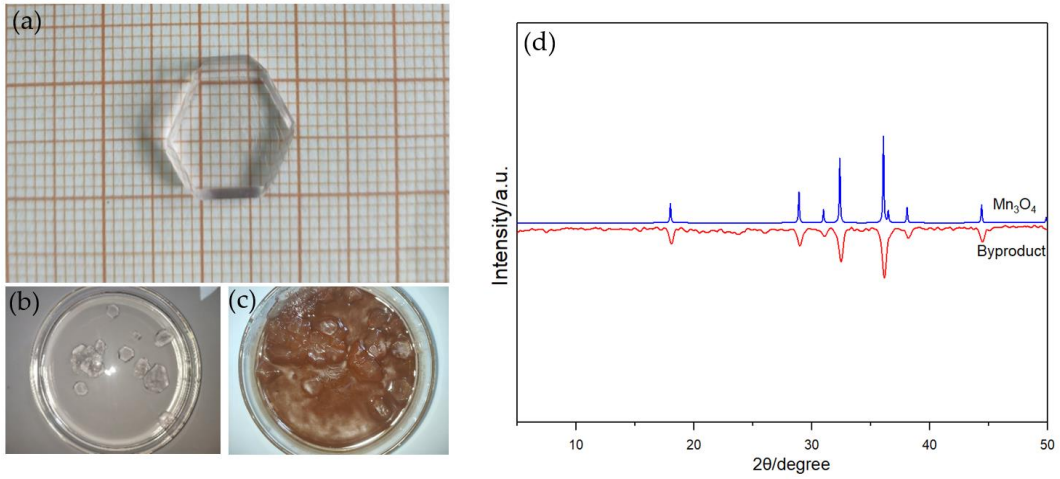

Fig. 1. (a) Crystal of $[Mn(C_6H_{12}N_4)_2(H_2O)_4][Mn(H_2O)_6][SO_4]_2\ 6H_2O$ with the size of 13mm × 12mm × 3mm. (b) Growth solution with sulfuric acid additive. (c) Growth solution without sulfuric acid additive. (d) Powder X-ray diffraction patterns for by-product (red) and Mn_3O_4 (blue)

2. 3 Structure determination

A transparent single crystal with dimensions of 0.25mm × 0.1mm × 0.1mm was mounted on a glass fiber for data collection on a MM007-Saturn724+ Small Molecule Single-Crystal X-ray Diffractometer operated at 45 kV and 16 mA using Mo*Kα* radiation. Lorentz polarization corrections and an empirical absorption were applied to the data. The structure was solved by direct methods and refined by full-matrix least-squares method with SHELXL (2018/3, Sheldrick, 2015) program package[20-22]. Residual electron densities in the solvent-accessible void due to disordered solvent molecules were treated with the PLATON SQUEEZE program[23]. The final R = 0.0423 and wR = 0.1186 (w = $1/[\sigma^2(F_o^2) + (0.0614P)^2]$, where $P = (F_o^2 + 2F_c^2)/3$), $(\Delta\rho)_{max}$ = 0.699 and $(\Delta\rho)_{min}$ = –0.571 e·Å^{-3}. Mercury and Crystal Maker were used to prepare the material for publication[24, 25].

3 RESULTS AND DISCUSSION

3. 1 PXRD pattern

Powder X-ray diffraction experiments were carried out to confirm the phase purity of the complex. As displayed in Fig. 2a, the single phase of the corresponding material can be seen from matching the peak position of the as-synthesized

PXRD pattern with the simulated peak pattern. For comparison, the PXRD of $[M(C_6H_{12}N_4)_2(H_2O)_4]$ $\{M(H_2O)_6\}\cdot 6H_2O$ (M = Zn, Ni and Co) was also presented in Fig. 2b. The diffraction peaks of the obtained material show a shift to low angles compared with that of Zn, Ni and Co complexes, corresponding with the fact that the title crystal has the largest unit cell volume (as listed in Table 1).

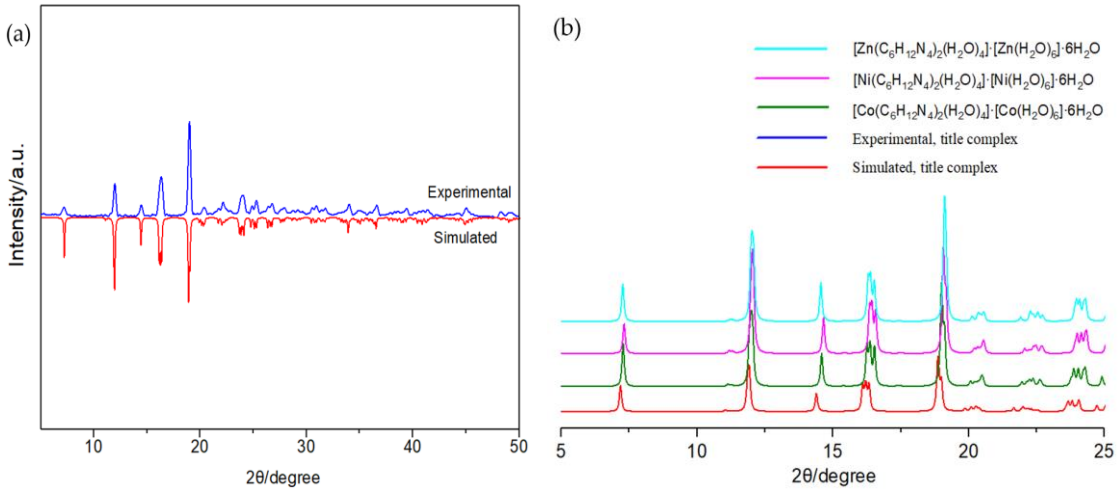

Fig. 2. (a) Powder X-ray diffraction patterns for the title complex (simulated, red; experimental, bule). (b) The selected diffraction peaks for the title complex and $[M(C_6H_{12}N_4)_2(H_2O)_4]$ $\{M(H_2O)_6\}$ $6H_2O$ (M = Zn, Ni and Co)

Table 1. Cell Parameters and Unit Cell Volume for $[M(C_6H_{12}N_4)_2(H_2O)_4]$ $\{M(H_2O)_6\}$ $6H_2O$ (M = Mn, Zn, Ni, Co)

M	*a*/Å	*b*/Å	*c*/Å	*α*/ °	*β*/ °	*γ*/ °	*V*/Å^3
Mn	9.339(8)	13.352(13)	16.321(13)	100.72(3)	90.10(1)	109.95(5)	1874.9(3)
Zn	9.255(1)	13.376(1)	16.085(1)	65.50(1)	89.76(1)	89.69(1)	1812.0(2)
Ni	9.253(1)	13.313(1)	16.037(1)	65.98(1)	89.79(1)	89.68(1)	1804.6(3)
Co	13.394(3)	16.077(3)	9.282(2)	89.71(2)	90.42(2)	114.02(2)	1825.6(7)

3. 2 Structure of the crystal

The perspective view of the molecular structure of the complex is illustrated in Fig. 3. Selected bond lengths and bond angles are reported in Table 2. It was different from some other manganese complexes where typically the Mn ions are coordinated in a single environment[26, 27]. This complex comprises two cationic complexes with different coordination geometry (distorted octahedron for $[Mn(C_6H_{12}N_4)_2(H_2O)_4]^{2+}$ and almost regular octahedron for $Mn(H_2O)_6^{2+}$) co-crystallizing with the sulfate anions. There are, besides, six crystalline water molecules in its molecule.

As can be seen in Fig. 3, the structure of $[Mn(C_6H_{12}N_4)_2(H_2O)_4]^{2+}$ units shows the Mn(II) ion is bound by four oxygen atoms from aqua ligands and two nitrogen atoms from the hexamethylenetetramine ligands. Atoms O(1), O(1a), O(2), O(2a) and Mn(1) occupy the equatorial plane, while N(1) and N(1a) locate at the axial positions to form a six-coordinated octahedral configuration. The axial angle O(1)–Mn(1)–N(1) is 89.48(6) °, which deviates from the ideal 90 °. By symmetry imposition, the two Mn(1)–N (Mn(1)–N(1), Mn(1)–N(1a)) bond lengths are equal to each other, 2.443(16) Å, significantly greater than that of Mn(1)–O (range from 2.136(15) to 2.138(16) Å). Based on the above discussion, the geometry around Mn(1) can be best described as a slightly distorted octahedral configuration. This distortion can be caused by steric and electronic effects of the ligands combined with the presence of the Mn(II) ion lone pair of electrons.

The hydrogen bonding analysis displayed in Fig. 4 reveals that $[Mn(C_6H_{12}N_4)_2(H_2O)_4]^{2+}$ cation is related to the neighboring groups in such a way that the spatial orientation of the groups is directed through the hydrogen bonding interactions. Atoms O from the $[Mn(H_2O)_6]^{2+}$ unit act as H-donor to the N atoms from the hexamethylenetetramine ligands, forming the hydrogen bonds O–H···N listed in Table 3. Moreover, classical intermolecular O–H···O hydrogen bonds between $[Mn(C_6H_{12}N_4)_2(H_2O)_4]^{2+}$ cations and SO_4^{2-} anions, $[Mn(H_2O)_6]^{2+}$ cations and lattice water molecules, as well as SO_4^{2-} anions and lattice water molecules, were also observed. Thus, the crystal structure of the complex shows an extensive hydrogen-bonding network interconnecting its constituent component and can be considered as a hydrogen-bonded assembly.

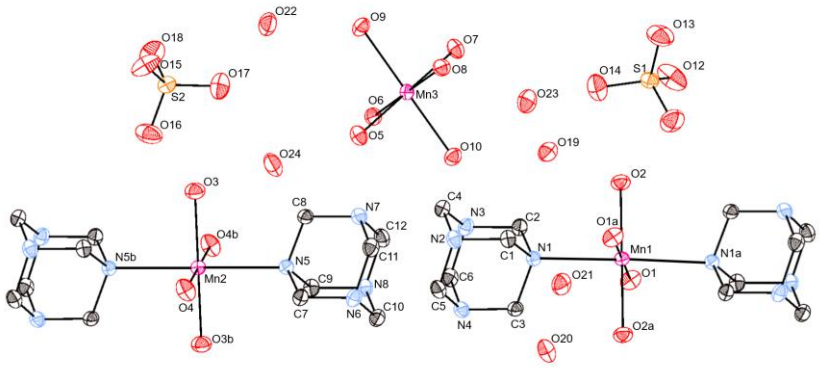

Fig. 3. View of the coordination environment of Mn(II) ion of the complex, shown with 30% probability displacement ellipsoids. H atoms have been omitted for clarity. Symmetry codes: (a) 2–*x*, 2–*y*, 2–*z*; (b) 1–*x*, –*y*, 1–*z*

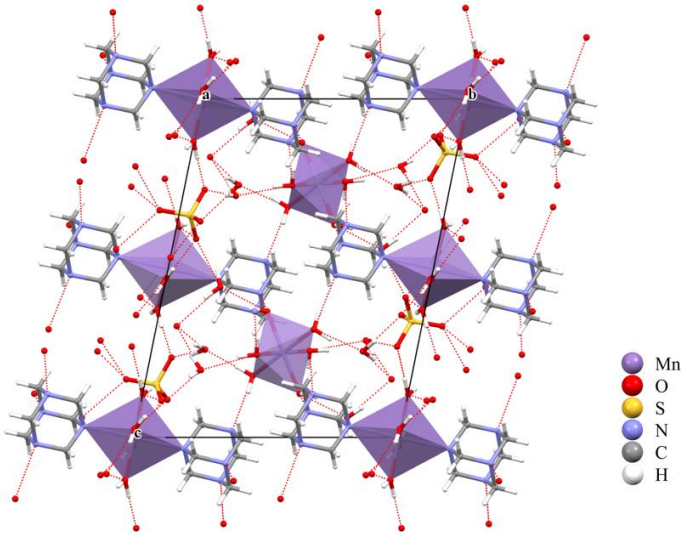

Fig. 4. Packing diagram for hydrogen bonds of the complex viewed along *a* axis

Table 2a. Selected Bond Lengths (Å)

Bond	Dist.	Bond	Dist.
Mn(1)–O(1)	2.136(15)	Mn(3)–O(5)	2.186(15)
Mn(1)–O(2)	2.138(16)	Mn(3)–O(6)	2.178(16)
Mn(1)–N(1)	2.443(16)	Mn(3)–O(7)	2.196(15)
Mn(2)–O(3)	2.144(16)	Mn(3)–O(8)	2.178(16)
Mn(2)–O(4)	2.129(16)	Mn(3)–O(9)	2.190(15)
Mn(2)–N(5)	2.443(16)	Mn(3)–O(10)	2.186(15)

Table 2b. Selected Bond Angles (°)

Angle	(°)	Angle	(°)
O(1)–Mn(1)–O(2)	93.41(7)	O(3)–Mn(2)–O(4)	94.40(7)
O(1)–Mn(1)–O(2)^a	86.59(7)	O(3)–Mn(2)–O(4)^b	85.60(7)
O(1)–Mn(1)–N(1)	89.48(6)	O(3)–Mn(2)–N(5)	90.37(6)
O(1)^a–Mn(1)–N(1)	89.48(6)	O(3)^b–Mn(2)–N(5)	89.63(6)
O(2)–Mn(1)–N(1)	87.33(6)	O(4)–Mn(2)–N(5)	92.24(6)
O(2)^a–Mn(1)–N(1)	92.67(6)	O(4)^b–Mn(2)–N(5)	87.76(6)

Symmetry codes: (a) 2–*x*, 2–*y*, 2–*z*; (b) 1–*x*, –*y*, 1–*z*

Table 3. Selected Hydrogen Bond Lengths and Bond Angles

D–H···A	d(D–H)/ Å	d(H···A)/ Å	d(D···A)/ Å	∠DHA/ °
O(5)[d]–H(5D)···N(2)[c]	0.86	2.04	2.864(2)	161
O(8)–H(8D)···N(4)[d]	0.86	2.03	2.826(2)	155
O(10)–H(10D)···N(3)	0.85	2.05	2.858(2)	158
O(9)–H(9D)···N(6)[d]	0.86	2.03	2.835(2)	158
O(6)–H(6D)···N(7)	0.86	2.07	2.868(2)	155
O(7)–H(7D)···N(8)[e]	0.86	2.04	2.864(2)	160
O(1)–H(1A)···O(15)[g]	0.85	1.82	2.667(2)	178
O(1)–H(1B)···O(13)[f]	0.85	2.06	2.804(3)	145
O(2)–H(2A)···O(11)	0.85	1.87	2.697(3)	164
O(2)–H(2B)···O(13)[h]	0.85	1.98	2.737(3)	148
O(3)–H(3C)···O(16)	0.85	1.86	2.693(2)	165
O(3)–H(3D)···O(18)[i]	0.85	1.98	2.762(3)	153
O(4)–H(4C)···O(12)[j]	0.85	1.77	2.618(3)	173
O(4)–H(4D)···O(18)[f]	0.85	2.22	2.994(3)	152

Symmetry codes: (a) 2 – *x*, 2 – *y*, 2 – *z*; (b) 1 – *x*, – *y*, 1 – *z*; (c) 1 – *x*, 1 – *y*, 2 – *z*; (d) –1 + *x*, *y*, *z*; (e) 1 – *x*, 1 – *y*, 1 – *z*; (f) 1 + *x*, *y*, *z*; (g) 1 + *x*, 1 + *y*, *z*; (h) 1 – *x*, 2 – *y*, 2 – *z*; (i) –*x*, –*y*, 1 – *z*; (j) *x*, –1 + *y*, *z*

3. 3 IR spectra

IR is effectively used to approve the structure determined by X-ray diffraction. Hexamethylenetetramine and obtained material were measured by the Vertex70 infrared spectrometer to qualitatively analyze the main functional groups in these compounds. Infrared data were collected in the range of 4000 ~ 400 cm^{-1}. Selected absorption peaks of hexamethylenetetramine and the obtained material are given in Table 4.

Table 4. Selected Absorption Peaks (cm^{-1}) of Hexamethylenetetramine and the Obtained Material

Compound	V_{CN}	V_{CH_2}	δ_{CH_2}	ρ_{CH_2}	V_{OH}	V_{SO_4}
Hexamethylenetetramine	1238, 1008	2945, 1370	1457	671	3458	–
Obtained material	1243, 1005	2965, 1381	1465	691	3416, 1658	1112, 615

Infrared spectra of hexamethylenetetramine and obtained material are quite similar. Absorption peaks at 2945, 1457 and 671 cm^{-1} for hexamethylenetetramine are assigned to C–H antisymmetric stretching, bending and rocking vibrations, respectively. For obtained material, the C–H vibration occurs at 2965, 1465 and 691 cm^{-1}, which is reasonable due to the presence of hexamethylenetetramine molecules in the structure of the complex. The C–N vibrations of obtained material are found at 1243 and 1005 cm^{-1}, and the clear shifts (1243 to 1238 cm^{-1}, 1005 to 1008 cm^{-1}) are observed compared to those of hexamethylenetetramine. These shifts are attributed to the coordination of hexamethylenetetramine to Mn(II) ions. In summary, the results of IR are in good agreement with the structure determination.

3. 4 Thermogravimetric analyses

Thermal analyses (Fig. 5), including thermal gravimetric analysis (TGA) and differential thermal analysis (DTA) measurements, were performed to examine the thermal stability of as-synthesized samples at a heating rate of 10 K/min from 30 to 800 °C in flowing N_2[28].

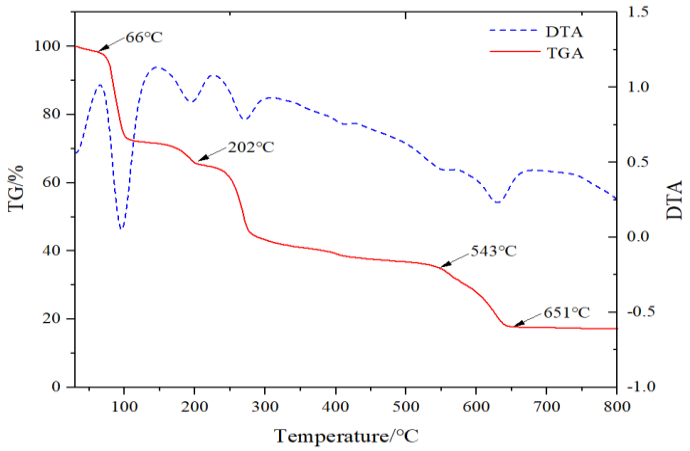

Fig. 5. TGA and DTA curves of the complex

The first step in the TGA of the compound agrees with the removal of six uncoordinated and ten coordinated water molecules (obsd. 33.41%, calcd. 33.09%), which appears between 66 and 202 °C. This is consistent with the fact that the complex is stable at room temperature. Further heating leads to the destruction of hexamethylenetetramine ligands. The second is attributed to the collapse of the framework, which falls in the range of 202～543 °C. A gradual weight-loss step of 17.49% (543～651 °C), corresponding to the decomposition of $MnSO_4$ into Mn_3O_4 (calcd. 17.17%). Above 651 °C, the final product of thermal decomposition, Mn_3O_4, is being formed. The experimental residual mass for the compound is close to the calculated ones, exp. 17.31%, calcd. 17.52%. DTA measurements give out the same results: the energy absorption peaks of the complex at 100 and 198 °C correspond to dehydration process, while the absorption energy peak corresponding to the skeleton decomposition is nearly 272 °C.

3. 5 Magnetic properties

Molar susceptibility (χ_M) measurements of the sample were performed in a temperature range of 2～300 K with an external magnetic field of 1000 Oe. Fig. 6 displays the plot of magnetic susceptibility data ($\chi_M T$, χ_M and χ_M^{-1}) versus temperature T. The value of $\chi_M T$ at 300 K is 11.49 $cm^3 \cdot K \cdot mol^{-1}$, slightly higher than the expected spin-only value of 8.76 $cm^3 \cdot K \cdot mol^{-1}$ for two uncoupled Mn(II) ions. Upon cooling, the $\chi_M T$ value first increased slowly to 11.73 $cm^3 \cdot K \cdot mol^{-1}$, and then decreased to 11.48 $cm^3 \cdot K \cdot mol^{-1}$ at 2 K. The observed behavior is the outcome of combined action of a variety of reasons, such as magnetic interaction between paramagnetic centers, the spin orbital coupling of Mn(II), the crystal field effect, magnetic interactions between molecules, and so on. In the temperature range of 2～300 K, the value of χ_M^{-1} increased linearly with the increase of T, indicating that the thermal evolution of $1/\chi_M$ obeys the Curie-Weiss law with C_m = 11.57 $cm^3 \cdot K \cdot mol^{-1}$ and θ = –0.430 K. The negative value of θ indicates that weak antiferromagnetic interactions take place between the adjacent manganese centers.

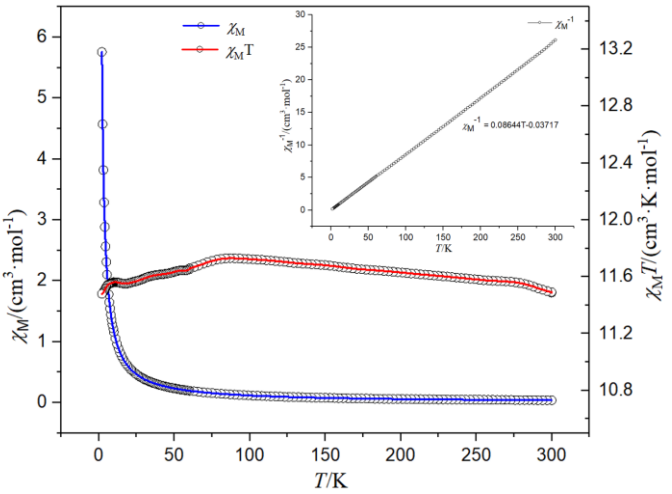

Fig. 6. Plots of temperature-dependent χ_M (bule), $\chi_M T$ (red) and χ_M^{-1} (black) under a 1 kOe dc field between 2 and 300 K for the complex

4 CONCLUSION

A novel manganese complex, $[Mn(C_6H_{12}N_4)_2(H_2O)_4][Mn(H_2O)_6][SO_4]_2\ 6H_2O$, was prepared and characterized. High quality single-crystals were obtained from solution with sulfuric acid additive by evaporation method. This compound comprises two different cationic complexes co-crystallizing with the sulfate anions. Magnetic studies indicate a relatively weak antiferromagnetic interaction between the Mn(II) centers. Comprehensive thermal analysis revealed compound a dehydration temperature of 66 ℃, which can conclude that the complex is an explorable magnetic material at room temperature. As far as future perspectives are concerned, we shall try to prepare other metal (such as Cu, Sr) complexes with hexamethylenetetramine as ligands.

REFERENCES

(1) Cahiez, G. R.; Duplais, C.; Buendia, J. J. Chemistry of organomanganese(II) compounds. *Chem. Rev.* **2009**, 109, 1434–1476.

(2) Yang, C.; Zhang, Z.; Lin, S. A review of manganese-based molecular magnets and supramolecular architectures from phenolic oximes. *Coordin. Chem. Rev.* **2015**, 289–290 (apr.), 289–314.

(3) Bartyzel, A.; Cristóvão, B.; Łyszczek, R. Crystal structure and thermal studies of coordination compounds. *Crystals* **2020**, 10, 1108.

(4) Zorina-Tikhonova, E.; Matyukhina, A.; Skabitskiy, I.; Shmelev, M.; Korchagin, D.; Babeshkin, K.; Efimov, N.; Kiskin, M.; Eremenko, I. Cobalt(II) complexes based on benzylmalonate anions exhibiting field-induced single-ion magnet slow relaxation behavior. *Crystals* **2020**, 10, 1130.

(5) Duboc, C. Determination and prediction of the magnetic anisotropy of Mn ions. *Chem. Soc. Rev.* **2016**, 47, 5834–5847.

(6) Thompson, L. K.; Dawe, L. N. Magnetic properties of transition metal (Mn(II), Mn(III), Ni(II), Cu(II)) and lanthanide (Gd(III), Dy(III), Tb(III), Eu(III), Ho(III), Yb(III)) clusters and [nxn] grids: isotropic exchange and SMM behaviour. *Coordin. Chem. Rev.* **2016**, 46, 13–31.

(7) Nandy, M.; Shit, S.; Rosair, G.; Gómez-García, C. J. Synthesis, characterization and magnetic studies of a tetranuclear manganese(II/IV) compound incorporating an amino-alcohol derived Schiff base. *Magnetochemistry* **2018**, 4, 57.

(8) Nagashima, H.; Asada, M.; Mino, H. Magnetic structure of manganese cluster in photosystem II investigated by electron paramagnetic resonance. *Biophy. Physicobio.* **2018**, 15, 45–50.

(9) Reed, G. H.; Poyner, R. R. Mn^{2+} as a probe of divalent metal ion binding and function in enzymes and other proteins. *Met. Ions Biol. Syst.* **2000**, 37, 183–207.

(10) Amirov, R. R.; Burilova, E. A.; Zhuravleva, Y. I.; Zakharov, A. V.; Ziyatdinova, A. B. NMR paramagnetic probing of polymer solutions using manganese(II) ions. *Polym. Sci. Ser. C+*. **2017**, 59, 133–140.

(11) Miao, Q.; Liu, W.; Thomas, K.; Blok, A.; Timmer, M.; Overhand, M.; Ubbink, M. A double-armed, hydrophilic transition metal complex as a paramagnetic NMR probe. *Angew. Chem. Int. Ed.* **2019**, 58, 13093–13100.

(12) Xiao, Y.; Ramchandra, P.; Liu, J.; Cong, M.; Zhang, Z.; Zhou, S. MRI contrast agents: classification and application. *Int. J. Mol. Med.* **2016**, 38, 1319–1326.

(13) Li, J.; Wu, C.; Hou, P.; Zhang, M.; Xu, K. One-pot preparation of hydrophilic manganese oxide nanoparticles as T-1 nano-contrast agent for molecular magnetic resonance imaging of renal carcinoma in vitro and in vivo. *Biosens. Bioelectron.* **2018**, 102, 1–8.

(14) Barandov, A.; Bartelle, B. B.; Williamson, C. G.; Loucks, E. S.; Lippard, S. J.; Jasanoff, A. Sensing intracellular calcium ions using a manganese-based MRI contrast agent. *Nat. Commun.* **2019**, 10, 897.

(15) Rummeny, E. J.; Torres, C. G.; Kurdziel, J. C.; Nilsen, G.; Beeck B, O. D.; Lundby, B. MnDPDP for MR imaging of the liver: results of an independent image evaluation of the European phase III studies. *Acta Radiol.* **1997**, 38, 638–642.

(16) Zhao, F. H.; Jia, X. M.; He, Y. C.; Huang, L. W.; Yan, X. Q.; Li, Z. L.; Li, J. X.; Feng, R.; You, J. M. Syntheses and magnetic properties of three transition metal complexes based on 4′-*p*-tolyl-2,2′:6′,2′′-terpyridine and SCN^-. *Polyhedron* **2019**, 173, 114–124.

(17) Kruszynski, R.; Sierański, T.; Świątkowski, M.; Zielak, M.; Wojciechowski, J.; Dzierżawska, M.; Lewiński, B. On the coordination behavior of the hmta toward zinc and cadmium cations in presence of sulfate(VI) and nitrate(V) anions. *J. Coord. Chem.* **2014**, 67, 1332–1352.

(18) Gao, S. M.; Xu, Z. H.; Ye, L. W.; Su, G. B.; Zhuang, X. X. Synthesis, crystal structure and properties of a coordination compound: $Ni(C_6H_{12}N_4)_2SO_4\ 4H_2O$. *Chin. J. Struct. Chem.* **2015**, 20, 1682–1688.

(19) Ammar, M. K.; Jouini, T.; Driss, A. Synthesis and structural characterization of dihexamethylenetetraminetetraaquocobalt(II) hexaaquocobalt(II) sulfate hexahydrate. *J. Chem. Crystallogr.* **2000**, 30, 265–268.

(20) Dolomanov, O. V.; Bourhis, L. J.; Gildea, R. J.; Howard, J. A. K.; Puschmann, H. OLEX2: a complete structure solution, refinement and analysis program. *J. Appl. Crystallogr*. **2010**, 42, 339–341.

(21) Sheldrick, G. M. Crystal structure refinement with SHELXL. *Acta Crystallogr. C Struct. Chem.* **2015**, 71, 3–8.

(22) Guzei, I. A. An idealized molecular geometry library for refinement of poorly behaved molecular fragments with constraints. *J. Appl. Crystallogr*. **2014**, 47, 806–809.

(23) Spek, A. L. Structure validation in chemical crystallography. *Acta Cryst. D Struct. Bio*. **2009**, D65, 148–155.

(24) Bruno, I. J.; Cole, J. C.; Edgington, P. R.; Kessler, M.; Macrae, C. F.; McCabe, P.; Pearson, J.; Taylor, R. New software for searching the Cambridge Structural Database and visualizing crystal structures. *Acta Crystallogr. B Struct. Sci.* **2002**, 58, 389–397.

(25) Yan, P.; Gao, Y.; Lu, Z.; Xue, G.; Zhao, Y. Application of crystal maker demo in crystallography and mineralogy teaching. *Guide Sci. Educ.* **2014**, 7S, 125–126.

(26) Feng, X.; Liu, J.; Li, J.; Ma, L. F.; Wang, L. Y.; Ng, S. W.; Qin, G. Z. Series of coordination polymers based on 4-(5-sulfo-quinolin-8-yloxy) phthalate and bipyridinyl coligands: structure diversity and properties. *J. Solid State Chem*. **2015**, 230, 80–89.

(27) Feng, X.; Shang, Y. P.; Wang, L. Y.; Hong, M. Z.; Fang, H. P.; Zhao, X.; Li, Z. J. A new manganese coordination polymer based on azobenzene tetracarboxylate and auxiliary pyridine ligand: synthesis, crystal structure and magnetic property. *Chin. J. Struct. Chem.* **2021**, 40, 217–224.

(28) Xiang, L.; Guo, X. F.; Li, X. X.; Hu, X. L. Temperature-dependent polymorphism in Co(II) coordination polymers from 5-nitroisophthalate and 1,3-bis(4-pyridyl)propane. *Chin. J. Struct. Chem*. **2013**, 11, 1680–1686.